

The albite fusion curve re-examined: New experiments and the high-pressure density and compressibility of high albite and NaAlSi₃O₈ liquid

TRAVIS J. TENNER,^{1,*} REBECCA A. LANGE,¹ AND ROBERT T. DOWNS²

¹Department of Geological Sciences, University of Michigan, 1100 N. University Avenue, Ann Arbor, Michigan 48109-1005, U.S.A.

²Department of Geosciences, University of Arizona, Tucson, Arizona 85721, U.S.A.

ABSTRACT

Experimental brackets on the melting temperature of high albite (NaAlSi₃O₈) were determined at 2.33 ± 0.03 GPa (1360–1370 °C) and 2.79 ± 0.03 GPa (1370–1389 °C) in a piston-cylinder apparatus. All run products that quenched to a glass were analyzed by Fourier-transform infrared spectroscopy and found to contain ≤ 500 ppm H₂O. In addition, new X-ray diffraction experiments on fully disordered albite are reported to 7.6 GPa; the fitted results lead to a zero-pressure bulk modulus (K_0) of 56.4 ± 0.7 and a pressure derivative (K'_0) of 3.9 ± 0.3 in a third-order Birch-Murnaghan equation of state. Revised values for the enthalpy and entropy of fusion of high albite at one bar and 1100 °C [$\Delta H_{T_f} = 64.5 \pm 2.1$ kJ/mol and $\Delta S_{T_f} = 47.0$ J/(mol·K)] are recommended on the basis of improved heat capacity equations for NaAlSi₃O₈ glass and liquid. On the basis of these new results on the fusion curve and thermodynamic data for high albite, the pressure dependence of the NaAlSi₃O₈ liquid compressibility (K'_0) is constrained to be 10.8 ± 1.5 in a third-order Birch-Murnaghan equation of state. The uncertainty in K'_0 of ± 1.5 contributes an error to melt density at 3 GPa (2.543 ± 0.010 g/cm³ at 1500 °C) of $\pm 0.4\%$.

Keywords: Compressibility measurements, albite, high-pressure studies, high-temperature studies, phase equilibria, thermodynamics

INTRODUCTION

Obtaining the density of fully polymerized silicate liquids at high pressure is a challenging task. Currently, most of our information on the density and compressibility of silicate liquids is derived from shock-wave (e.g., Rigden et al. 1989) and/or sink-float (Agee and Walker 1993) experiments, which are not well suited for viscous liquids such as molten NaAlSi₃O₈. An alternative approach is to use fusion curve analysis, which is a comparison between phase equilibrium experiments on the congruent melting reaction of a mineral at pressure and the calculated melting reaction from measured thermodynamic properties. It thus has the potential to constrain the value of a single thermodynamic property (e.g., the liquid density at pressure) for which direct, independent measurements are not feasible. This was the approach taken by Lange (2003, 2007) to constrain the pressure dependence of the melt compressibility, $K'_0 (= dK_{T,0}/dP$, where $K_{T,0} = 1/\beta_{T,0}$) for liquid NaAlSi₃O₈ and KAlSi₃O₈, respectively.

Lange (2003) discussed the thermodynamic data used to calculate the fusion curve of albite and, based on a comparison with four previous experimental phase equilibrium studies (Birch and LeComte 1960; Boyd and England 1963; Boettcher et al. 1982; Nekvasil and Carroll 1996) of the albite melting reaction, estimated that the K'_0 of NaAlSi₃O₈ liquid has a minimum value of 10. However, each experimental study lacked one or more key components essential to a robust determination of the fusion curve: (1) documentation of dissolved H₂O in the quenched glass

run products; (2) a detailed thermal gradient determination and pressure calibration prior to experiments; and (3) characterization of crystalline starting material to be sure it was fully disordered, high albite. To tightly bracket the K'_0 value for liquid NaAlSi₃O₈, the goal of this study is to locate the fusion curve of albite in P - T space through a series of piston-cylinder experiments, and address each component described above. In addition, we re-evaluate the thermodynamic data used in the calculation of the fusion curve and present new experiments on the compressibility of high albite.

THERMODYNAMIC CALCULATION OF THE FUSION CURVE

The equation used to calculate the melting curve for albite at temperature and pressure is:

$$\Delta H_{T_f} + \int_{T_f}^T \Delta C_p(T) dT - T \left(\Delta S_{T_f} + \int_{T_f}^T \frac{\Delta C_p(T)}{T} dT \right) = - \int_1^P \Delta V_T(P) dP \quad (1)$$

where T_f is the one-bar melting temperature of crystalline albite, ΔH_{T_f} is the enthalpy of the liquid minus that of the solid at T_f , ΔS_{T_f} is the entropy of the liquid minus that of the solid at T_f , $\Delta C_p(T)$ is the heat capacity of the liquid minus that of the solid, and $\Delta V_T(P)$ is the volume of the liquid minus that of the solid. Among the thermodynamic data required, the only unknown is the liquid K'_0 , which is needed to calculate the albite fusion curve above 1 GPa (Lange 2003).

To determine the K'_0 of NaAlSi₃O₈ liquid, the third-order Birch-Murnaghan equation of state (Birch 1978) is used, which models the volume of silicate liquids to high pressure (tens of

* E-mail: tenn0047@umn.edu

GPa) remarkably well (e.g., Stixrude and Bukowinski 1990a). The third-order form is:

$$P = \frac{3}{2} K_{T,0} (R^{7/3} - R^{5/3}) \left[1 - \frac{3}{4} (4 - K'_0) (R^{2/3} - 1) \right] \quad (2)$$

Where $R = V_{T,0}/V_{T,P}$, $V_{T,0}$ is the volume at temperature and zero pressure (1 bar), $V_{T,P}$ is the volume at temperature and pressure, $K_{T,0}$ is the bulk modulus ($K_{T,0} = 1/\beta_{T,0}$, where $\beta_{T,0}$ is the isothermal compressibility) at zero pressure, and K'_0 is the pressure dependence of the bulk modulus ($dK_{T,0}/dP$) at zero pressure. With this equation, K' is not constrained to be independent of pressure, and the implied value of K'' (dK'/dP) is given in Anderson (1995):

$$K'' = -\frac{1}{K_{T,0}} \left[(3 - K'_0)(4 - K'_0) + \frac{35}{9} \right] \quad (3)$$

The values for the thermodynamic properties used in Equation 1 are summarized in Table 1; most were previously reviewed and recommended by Lange (2003). At that time, there were no high-pressure X-ray diffraction experiments on fully disordered albite, and so the compressibility data for low albite (Downs et al. 1994) were used instead. However, because compressibility measurements on sanidine and microcline indicate that Al/Si disorder affects the bulk modulus (Hackwell 1993; Angel et al. 1988), direct compressibility data for high albite are required. In this study, new X-ray data are presented for fully disordered albite to 7.6 GPa. In addition, the value for the enthalpy of fusion (ΔH_{T_f}) for albite at its one-bar melting temperature (1373 K) is re-examined in greater detail than previously done by Lange (2003), and a revised estimate for ΔH_{T_f} is provided below. These new values are used in the thermodynamic calculation of the fusion curve.

The compressibility of high albite to 7.6 GPa

A single crystal of low albite from Crete was obtained from the Smithsonian Institution (specimen no. U.S.N.M. 123519) and heated at 1355 K for seven months. The study of the compressibility of low albite by Downs et al. (1994) used an unheated fragment from the same crystal. Cell parameters were obtained in air (Table 2) that corresponds to complete Al/Si disorder according to Figure 7.6 from Smith and Brown (1988). The crystal ($70 \times 70 \times 40 \mu\text{m}^3$) was mounted in a 4-pin diamond anvil cell with Be seats, 600 μm culets on the diamonds, 300 μm diameter hole in a 250 μm thick T-301 Martensitic steel gasket that was pre-indented to 90 μm , with a 4:1 mixture of methanol-ethanol as a pressure medium. The pressure was obtained by fitting the

TABLE 1. Summary of thermodynamic data used to calculate albite fusion curve

Parameter	Value	Reference
T_f	1373 K	Boettcher et al. (1982)
$\Delta H_{fus}(T_f)$	64.5 ± 2.1 kJ/mol	This study
$\Delta S_{fus}(T_f)$	47.0 J/(mol·K)	This study
C_p crystal	$393.64 - 2415.5T^{-0.5} - 7.8928 \cdot 10^5 T^{-2} + 1.07064 \cdot 10^9 T^{-3}$	Berman (1988)
C_p liquid	359 ± 4 J/(mol·K)	This study
V_{298K} crystal	100.27 cm ³ /mol	This study
$\alpha(T)$ crystal	$0.2455 \cdot 10^{-4} + 0.7621 \cdot 10^{-8} (T - 298) \text{ K}^{-1}$	Fei (1995)
K_0 crystal	56.4 ± 0.7 GPa	This study
K'_0 crystal	3.9 ± 0.3	This study
$V(T)$ liquid	$112.72 + 0.00382 (T - 1373) \text{ cm}^3/\text{mol}$	Lange (1996)
$\beta_0(T)$ liquid	$5.78 + 0.00026 (T - 1773) \cdot 10^{-2} \text{ GPa}^{-1}$	Kress et al. (1988)
K'_0 liquid	10.8 ± 1.5	This study

fluorescence spectra of an included ruby chip according to Mao et al. (1978). The positions of 25 high intensity peaks were carefully determined from the 8-peak centering algorithm of King and Finger (1979), and cell parameters were refined as a function of pressure to 7.6 GPa and are reported in Table 2. The errors of the unit-cell volumes are about five times smaller than those reported by Downs et al. (1994) in their high-pressure study of low albite because of improved centering techniques that include fitting each scan to a pair of Gaussian functions that correspond to $\text{MoK}\alpha 1$ and $\text{K}\alpha 2$ radiation (Angel et al. 2000). The errors associated with the length of the b axis are larger than those for the other cell edges because the crystal was mounted with b^* roughly parallel to the DAC axis.

The weighted volume and pressure data in Table 2 were fitted to a third-order Birch-Murnaghan equation of state that gave a zero pressure volume, $V_0 = 665.87 \pm 0.04 \text{ \AA}^3$, a zero pressure bulk modulus, $K_0 = 56.4 \pm 0.7$ GPa, and a pressure derivative, $K'_0 = 3.9 \pm 0.3$. Thus, the disordered state of albite is slightly less compressible than the ordered state, where the bulk modulus was found to be 54 ± 1 GPa by Downs et al. (1994). In contrast, the bulk modulus of the ordered K-feldspar (microcline) is $K_0 = 63 \pm 2$ GPa (Hackwell 1993), whereas it is $K_0 = 57 \pm 1$ GPa for the disordered K-feldspar (sanidine) (Angel et al. 1988). Figure 1 shows the P - V data and fitted curves for these four phases. Furthermore, Hackwell and Angel (1992) showed that ordered anorthite, $Q_{OD} = 0.92$ ($K_0 = 83 \pm 1$ GPa) is also less compressible than disordered anorthite, $Q_{OD} = 0.78$ ($K_0 = 79.8 \pm 0.3$ GPa). Thus the increase in the bulk modulus with disorder for albite is in the opposite sense of the other feldspar minerals.

The new equation of state for high albite vs. that for low albite (Downs et al. 1994) in Equation 4 leads to a calculated melting temperature at 3 GPa that is ~ 1 degree lower.

The enthalpy and entropy of fusion

Different values for the enthalpy of fusion of albite, ΔH_{T_f} , are reported in the literature: 62.8 ± 2.1 kJ/mol at 1373 K (Stebbins et al. 1983) and 64.5 ± 3.0 kJ/mol at 1393 K (Richet and Bottinga 1984). Because both estimates are derived from a nearly identical

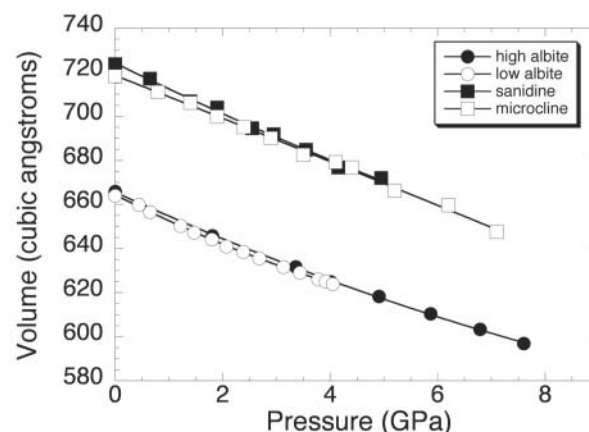


FIGURE 1. The unit-cell volume for high albite obtained in this study by X-ray diffraction experiments in a diamond cell anvil to 7.6 GPa. Also shown are variations in unit-cell volume for low albite, microcline, and sanidine from Downs et al. (1994), Hackwell (1993), and Angel et al. (1988), respectively.

TABLE 2. Cell parameters for fully disordered albite (NaAlSi₃O₈)

	P (GPa)	a (Å)	b (Å)	c (Å)	α (°)	β (°)	γ (°)	V (Å ³)
P0	0	8.1520(3)	12.8682(5)	7.1074(2)	93.497(3)	116.450(2)	90.275(3)	665.87(4)
P1	1.81(3)	8.0263(5)	12.7867(7)	7.0546(4)	93.706(10)	116.539(4)	90.418(9)	645.84(6)
P3	3.36(3)	7.9336(4)	12.7264(13)	7.0159(4)	93.774(10)	116.545(3)	90.583(11)	631.69(7)
P4	4.01(3)	7.8884(4)	12.6945(11)	6.9972(3)	93.782(8)	116.531(3)	90.637(8)	624.89(6)
P5	4.91(3)	7.8436(3)	12.6649(11)	6.9784(3)	93.796(8)	116.517(3)	90.691(7)	618.26(6)
P6	5.87(3)	7.7876(3)	12.6295(11)	6.9553(3)	93.755(8)	116.467(3)	90.775(8)	610.37(6)
P7	6.79(3)	7.7387(4)	12.5961(9)	6.9347(4)	93.769(8)	116.424(4)	90.840(8)	603.32(6)
P8	7.60(3)	7.6933(3)	12.5674(8)	6.9140(3)	93.804(8)	116.350(3)	90.909(8)	596.93(5)

set of primary measurements, a detailed examination is required to understand the difference in reported values for ΔH_{T_f} .

Because NaAlSi₃O₈ liquid quenches to a glass (and not 100% crystals) during a drop calorimetric experiment, direct determination of ΔH_{T_f} from these experiments is not possible. Instead, ΔH_{T_f} is calculated from measurements of the heat of vitrification ($\Delta H_{T_g}^{vit}$; difference in enthalpy between glass and crystal) by solution calorimetry at the temperature of the solution (T_s), and then taken to high temperature by integration of the heat capacity functions for crystal, glass, and liquid as shown in the following equation:

$$\Delta H_{T_g}^{fvs} = \Delta H_{T_g}^{vit} + \int_{T_g}^{T_s} [C_p^{\text{glass}}(T) - C_p^{\text{crystal}}(T)]dT + \int_{T_g}^{T_s} [C_p^{\text{liquid}}(T) - C_p^{\text{crystal}}(T)]dT \quad (4)$$

Thus, the data required to calculate the enthalpy of fusion for albite are (1) the enthalpy of vitrification for NaAlSi₃O₈ by solution calorimetry ($\Delta H_{T_g}^{vit}$); (2) the heat capacity of NaAlSi₃O₈ crystal, glass, and liquid; (3) the glass transition temperature for the glass used in the solution calorimetry experiments (T_g); and (4) the melting temperature of albite at one bar (T_f).

Both Stebbins et al. (1983) and Richet and Bottinga (1984) used the heat of vitrification for albite (51.89 kJ/mol at 985 K) reported by Navrotsky et al. (1980), and both use the same heat capacity equation for crystalline albite, namely that of Hemingway et al. (1981). The differences between their two calculations include (1) the heat capacity of NaAlSi₃O₈ glass; (2) the glass transition temperature; (3) the heat capacity of NaAlSi₃O₈ liquid; and (4) the one-bar melting temperature. The effect of each of these differences on the calculated enthalpy of fusion is quantified below. In addition, the effect of using two different equations for the heat capacity of crystalline albite (Hemingway et al. 1981; Berman 1988) is also examined.

The effect of glass C_p

The heat capacity of NaAlSi₃O₈ glass has been measured by differential scanning calorimetry by Robie et al. (1978), Krupka et al. (1979), and Stebbins et al. (1982) from 300–1000 K. The best available heat capacity equation for glass is that of either Stebbins et al. (1983) or Richet (1987); they are nearly identical and lead to a difference in calculated values of ΔH_{T_f} of <0.2 kJ/mol. In contrast, the glass heat capacity equation used by Richet and Bottinga (1984) extrapolates to low values above 1000 K (Fig. 2), which in turn leads to a decrease in ΔH_{T_f} of ~0.8 kJ/mol compared to the equation of Stebbins et al. (1983).

Choice of glass transition temperature

The glass transition temperature that should be applied in Equation 4 is that for the glass used in the solution calorimetry experiments to obtain the heat of vitrification. The NaAlSi₃O₈ glass employed by Navrotsky et al. (1980) was quenched from a liquid heated to 1923 K (1650 °C). Although the glass transition tem-

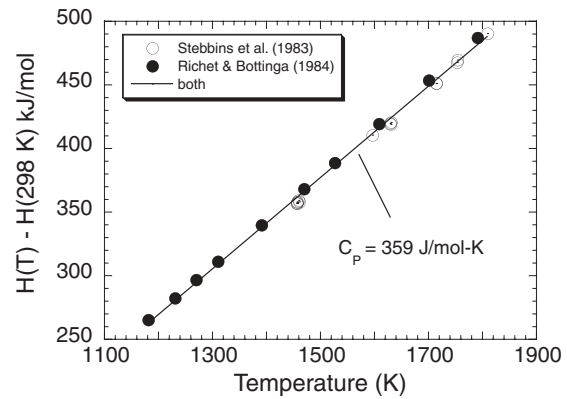


FIGURE 2. Enthalpy vs. temperature for NaAlSi₃O₈ liquid and glass from the drop calorimetry experiments of Stebbins et al. (1983) and Richet and Bottinga (1984). A linear fit to the data from both studies leads to a temperature-independent liquid heat capacity of 359 ± 4 J/(mol·K).

perature of this glass was not directly determined by Navrotsky et al. (1980), NaAlSi₃O₈ glass quenched in an identical manner (from 1923 K) was shown to have a glass transition temperature (T_g) of 1092 K, as measured by dilatometry (Lange 1996). Therefore, heat-treatment of the NaAlSi₃O₈ glass by Navrotsky et al. (1980) for 1.5–2.5 h at 985 K, more than 100 degrees below T_g and thus well within the glass region, is unlikely to have changed the value of T_g . Therefore, the appropriate value of T_g to employ in Equation 4 is a value near 1092 K, which is very close to the value of T_g (1096 K) reported by Richet and Bottinga (1984) in their drop calorimetry experiments. In contrast, Stebbins et al. (1983) used a value for T_g of 1190 K, which is likely too high for the NaAlSi₃O₈ glass used by Navrotsky et al. (1980), as discussed above. The difference in using 1096 vs. 1190 K for T_g in Equation 4, with all other parameters unchanged, leads to a difference in ΔH_{T_f} of ~3.2 kJ/mol, with the lower value for T_g (1096 K) leading to a higher ΔH_{T_f} value. An uncertainty in T_g of ± 25 K leads to an uncertainty in ΔH_{T_f} of ± 0.8 kJ/mol.

Effect of liquid C_p

Another critical input to the calculation of ΔH_{T_f} is the liquid heat capacity. Stebbins et al. (1983) used a temperature-independent value of 369 J/mol, whereas Richet and Bottinga (1984) used a temperature-dependent value that ranges from ~340 to ~360 J/(mol·K) between 1096 K (T_g) and 1373 K (T_f). This difference in liquid heat capacity, with all other parameters unchanged, leads to a difference in ΔH_{T_f} of ~3.7 kJ/mol at 1373 K. However, a linear fit to the drop calorimetric data of Richet and Bottinga (1984), shown in Figure 2, leads to a temperature-independent

liquid C_p of 364 J/(mol·K). The difference in liquid heat capacity between 364 J/(mol·K) and the temperature-dependent form given by Richet and Bottinga (1984), with all other parameters unchanged, leads to a difference in ΔH_{T_f} of ~ 3.1 kJ/mol. The value recommended in this study is 359 ± 4 J/(mol·K), based on a linear fit to the data of both Richet and Bottinga (1984) and Stebbins et al. (1983) between 1182 and 1810 K (Fig. 2).

Choice of one-bar melting temperature

The final difference between the two calculations is the choice of one-bar melting temperature: 1373 K by Stebbins et al. (1983) and 1393 K by Richet and Bottinga (1984). As reviewed by Lange (2003), the fully reversed experiments of Boettcher et al. (1982) constrain the melting temperature at 1373 ± 3 K. A difference of 20 degrees leads to a difference in ΔH_{T_f} of ~ 0.7 kJ/mol for a liquid C_p of 359 J/(mol·K).

Effect of crystalline C_p

Both Stebbins et al. (1983) and Richet and Bottinga (1984) used the same heat capacity equation for crystalline albite, namely that of Hemingway et al. (1981). Therefore, the difference in their results does not arise from this parameter. However, as discussed by Lange (2003), the heat capacity equation for albite of Berman (1988) extrapolates to high temperature in a more realistic manner and is therefore preferred. The difference in the calculated value of ΔH_{T_f} that arises from using the equation of Hemingway et al. (1981) vs. that of Berman (1988) (for a T_g of 1096 K and a T_f of 1373 K) is 0.6 kJ/mol, with the Berman (1988) equation leading to the larger ΔH_{T_f} .

Recommended values for ΔH_{T_f} and ΔS_{T_f} at 1373 K

Figure 3a summarizes the data used by Stebbins et al. (1983), whereas Figure 3b illustrates those used by Richet and Bottinga (1984). In this study, the values for ΔH_{T_f} reported by Stebbins et al. (1983) and Richet and Bottinga (1984) (62.8 ± 2.1 and 62.1 ± 1.2 kJ/mol, respectively) for the input parameters shown in Figure 3 are closely recovered (62.5 and 61.8 kJ/mol, respectively). Note that although Richet and Bottinga (1984) report the value of 62.1 kJ/mol in their Table 4 for the parameters in Figure 3b, their selected value for ΔH_{T_f} is higher (64.5 kJ/mol).

Figure 3c summarizes the best available thermodynamic data to use in Equation 4 to calculate ΔH_{T_f} . When the heat of vitrification of Navrotsky et al. (1980) is used, along with the best available heat capacity equations for albite (Berman 1988), $\text{NaAlSi}_3\text{O}_8$ glass (Richet 1987) and $\text{NaAlSi}_3\text{O}_8$ liquid (a linear fit to the data of both Stebbins et al. 1983; Richet and Bottinga 1984), and when the appropriate glass transition temperature is used ($\sim 1096 \pm 25$ K; that for the $\text{NaAlSi}_3\text{O}_8$ glass used in the solution calorimetry experiments), then the calculated heat of fusion for albite is 64.5 ± 2.1 kJ/mol at 1373 K. This value is ~ 1 kJ/mol higher than that used by Lange (2003) and leads to a calculated melting temperature that is ~ 4 degrees lower at 3 GPa (with all other parameters unchanged in Eq. 1).

The entropy of fusion, ΔS_{T_f} , is calculated from ΔH_{T_f} at the fusion temperature from the relationship: $\Delta H_{T_f} - T_f \Delta S_{T_f}$. For a one-bar melting temperature of 1373 and a ΔH_{T_f} value of 64.5 ± 2.1 kJ/mol, the resultant value for ΔS_{T_f} is 47.0 J/(mol·K). These are the recommended values for ΔH_{T_f} and ΔS_{T_f} at 1373 K, and

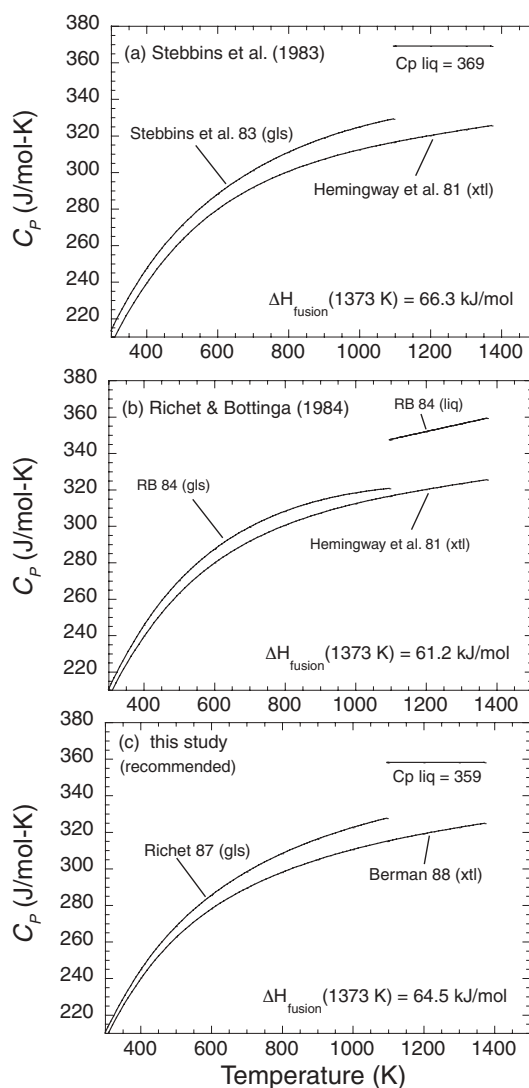


FIGURE 3. An illustration of the C_p equations for high albite, $\text{NaAlSi}_3\text{O}_8$ glass and liquid used by (a) Stebbins et al. (1983), (b) Richet and Bottinga (1984), and (c) recommended in this study for the respective calculations of the enthalpy of fusion of albite at one bar from Equation 4 in the text.

they are used in the fusion curve calculation discussed below. The uncertainty of ± 2.1 kJ/mol in ΔH_{T_f} leads to an uncertainty in the calculated fusion temperature of ± 8 degrees at 3 GPa. For an error analysis of all other thermodynamic data used in Equation 1 and listed in Table 1, see Lange (2003).

PREVIOUS PHASE EQUILIBRIA WORK

There have been four phase-equilibrium studies on the melting reaction of crystalline albite at pressures ≥ 10 kbar (Birch and LeComte 1960; Boyd and England 1963; Boettcher et al. 1982; Nekvasil and Carroll 1996). The fusion curve is limited to pressures ≤ 3.3 GPa by the albite = jadeite + quartz reaction (Holland 1980). Below, a brief review of each previous experimental study is provided along with an outline of some remaining questions regarding the melting reaction of albite.

Study of Birch and LeComte (1960)

The experiments of Birch and LeComte (1960) were performed in an internally heated gas vessel with argon gas as the pressure medium, thus allowing the pressure to be precisely and accurately known and minimizing H₂O in the system. Seven of their nine experiments had a starting material of crystalline albite; however it is unclear if it was low or high albite. Anovitz and Blencoe (1999) noted that low albite will melt metastably at lower temperatures than high albite. All seven gave “no-reaction” results, which may be difficult to interpret. No reaction with a starting material of crystalline albite might mean that it was in the crystalline stability field at the *P-T* conditions of the experiment, or it might have remained crystalline because of sluggish kinetics. Run durations of these experiments ranged from 0.2–5.75 h. The other two experiments by Birch and LeComte employed NaAlSi₃O₈ glass as the starting material. In these two runs, crystallization occurred within 4 and 2 h, respectively, which constrains the melting temperature of albite to be ≥ 1210 °C at 1.22 GPa, and ≥ 1279 °C at 1.51 GPa.

Study of Boyd and England (1963)

The experiments of Boyd and England (1963) also provide constraints on the minimum temperatures for the albite fusion curve. The starting material was NaAlSi₃O₈ glass, and experiments were conducted with a 1.27 cm piston-cylinder apparatus using talc/boron nitride (BN) as the pressure medium. Experimental run durations ranged from 20–60 min. Twenty-five degree brackets on the half-reversal were determined at nominal pressures of 1.08 GPa (1225–1250 °C), 1.79 GPa (1300–1325 °C), 2.51 GPa (1350–1375 °C), and 3.23 GPa (1400–1425 °C).

Talc/BN assemblies require a pressure correction, and Boyd and England (1963) carried out calibrations at both room temperature and elevated temperatures. Using bismuth, thallium, and cesium phase transitions at room temperature, they found the friction with the piston advancing to be 13% of the nominal pressure. At elevated temperatures they used the quartz-coesite phase transition, and determined the pressure correction to be 8% of the nominal pressure. Boyd and England (1963) noted that the furnace cells used for the quartz-coesite experiments contained a considerable amount of porous ceramic. Upon pressurization the porous ceramic collapsed, and the talc extruded into cracks and chips in the pressure vessel. Thus, the piston was continually advanced to maintain a constant pressure during their experiments. However, they used a different cell assembly for the albite melting experiments where the ceramic pore volume was reduced, and they noted that piston motion was reduced extensively after the first 1–2 min of their runs. Based on the lack of piston advancement, their pressure correction was uncertain, and they therefore assumed no pressure correction for their experiments. However, Bohlen et al. (1980) later demonstrated through a pressure calibration against the melting curve of LiCl, that talc/BN assemblies require a negative 6% correction.

An additional concern is that talc/boron nitride assemblies dehydrate at high temperatures, which can lead to hydrogen diffusion into the platinum capsules (Tuttle and Bowen 1958). There was no documentation on how much water may have contaminated the experimental charges of Boyd and England (1963), which will depress the melting temperature. Therefore, only the

experiments where the run products are crystalline can be used to constrain the minimum melting temperature of albite.

Study of Boettcher et al. (1982)

Boettcher et al. (1982) also determined the fusion curve of albite using a 1.27 cm diameter (for 3 GPa experiments) and a 2.54 cm diameter piston-cylinder apparatus. The advantages of their study are that full-reversals were determined and the crystalline starting material was well characterized. To avoid water contamination, their furnace assemblies contained no hydrous parts such as talc or pyrophyllite. Instead the assemblies consisted of KBr, NaCl, silica glass, and BN, which also had the advantage of having no pressure correction applied to the nominal pressure. The starting materials were sealed into 1.6 mm diameter platinum capsules which were surrounded by hematite and sealed into 3 mm platinum tubing to further prevent water contamination. Experimental runs were 3–24 h in duration. The results of Boettcher et al. (1982) place the melting curve of albite 50–70 °C lower than the experiments of Birch and LeComte (1960) and Boyd and England (1963). The likely explanation for lower than expected results is that water contaminated their samples, despite their best efforts at keeping their runs dry. None of the samples of Boettcher et al. (1982) were directly measured for water content; however two lines of evidence that suggest water contamination occurred. First, there are the water concentrations measured by Fine and Stolper (1985), both on albite glass samples provided by A.L. Boettcher (0.20 and 0.49 wt% H₂O) and on samples they synthesized in a piston cylinder for 1–3 h (≤ 0.89 wt% H₂O) using the same cell assembly and drying technique of Boettcher et al. (1982). Second, the experiments of Boettcher et al. (1982) in the NaAlSi₃O₈ liquid stability field did not quench to a glass, but instead to quench crystals. This is in contrast to the findings of Birch and LeComte (1960), Boyd and England (1963), and Nekvasil and Carroll (1996), who all recovered glasses from their experiments and noted the ease with which albite liquid quenches to a glass. It is likely that the presence of water, which reduces melt viscosity, may have prevented glass formation in the Boettcher et al. (1982) experiments.

Study of Nekvasil and Carroll (1996)

The most recent study of the albite melting reaction was performed by Nekvasil and Carroll (1996). Their experiments were performed in a piston-cylinder apparatus, and were conducted using a BN/NaCl pressure medium. A pressure calibration using the anhydrous reaction Mg-cordierite = sapphirine + quartz showed that no pressure correction was required. Samples containing crystalline albite as the starting material were held at a pressure of 1.13 GPa and 1400 °C for 24 h to ensure melting had occurred before rapidly reducing the temperature to its final value. Experiments were then held for an additional 4 days. Four experiments were performed, and the results are as follows: at 1230 and 1240 °C the run products were glass, whereas at 1200 and 1225 °C the run products were crystalline. This constrains a five degree bracket of 1225–1230 °C on the minimum melting temperature of albite, because the H₂O in their quenched glasses was not determined. The bracket at 1.13 GPa is approximately 25 °C higher than that of Boettcher et al. (1982) at a similar pressure. However, it is within the temperature brackets of the results of

Birch and LeComte (1960) as well as Boyd and England (1963), if no pressure correction is applied to the latter study.

NEW PHASE EQUILIBRIUM EXPERIMENTS

All experiments were carried out in a piston-cylinder apparatus with 1.27 cm diameter furnace assemblies and pistons. Figure 4 shows the BaCO₃-MgO-graphite pressure assembly. Temperature was measured with Pt/Pt₉₀Rh₁₀ (type S) thermocouple, with an error of ± 2 °C over the temperature range of the experiments. No correction for the effect of pressure on emf was applied. Pressure was measured with a 30.5 cm Heise gauge, which has a precision of $\pm 0.1\%$ of the measured oil pressure.

Hotspot determination and the thermal gradient down length of sample capsule

The location of the hotspot and the thermal gradient down the length of the sample capsule were mapped out at 2.0 GPa (nominal) through several experiments at different set points (300–1400 °C; Tenner 2005) where the temperature readings of two thermocouples were made: one in a fixed position to control the set-point, whereas the other was moved as a function of distance from the base plug. At the highest set-point temperature (1400 °C), the furnace assemblies were subjected to pressures ranging from 2.0 to 3.0 GPa (nominal), and it was found that pressure had no effect on the temperature difference measured between the two thermocouples. A polynomial (relating temperature to distance from the base plug) was fitted to the data at each set-point temperature, which had R^2 values ranging from 0.9996 to 1 (Tenner 2005). From the curves, the hotspot was located, and the temperature gradient was mapped.

An example is shown in Figure 5 for a hotspot temperature of 1398 °C at 2 GPa (nominal). The measured thermal gradient permits a 3 mm long Pt capsule to be positioned so that when the

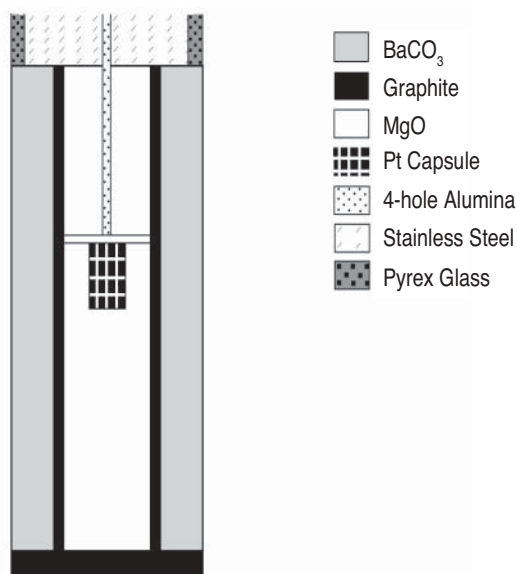


FIGURE 4. Schematic diagram of the pressure assembly in the piston-cylinder apparatus. The assembly dimensions are BaCO₃ length = 30 mm; graphite furnace length = 30 mm; solid MgO length = 17.5 mm; MgO disk = 0.5 mm; drilled MgO length = 12 mm; capsule length = ~ 3.5 mm; capsule width = ~ 3 mm.

hotspot is in the center, there is a gradient of only 9 degrees along the capsule length. Alternatively, a 3 mm long Pt capsule can be positioned so that the hotspot is at the top of the capsule, which gives rise to a thermal gradient of ~ 32 degrees down the length of the capsule, but also ensures a steadily declining temperature from top to bottom. The latter configuration was chosen for the experiments in this study to permit unambiguous interpretation of the quenched run products.

Pressure calibration

The pressure correction for the BaCO₃-MgO pressure assembly used in this study (Fig. 4) was determined by bracketing the melting temperature of NaCl (99.997% purity) at a nominal pressure of 2 GPa. The strategy employed for this highly fluid liquid that does not quench to a glass is to place a small Pt-Rh bead on top of tightly packed crystalline NaCl powder, which is enclosed in a 3 mm diameter Pt capsule. Prior to sealing, the NaCl powder is heated at 450 °C for ≥ 2 h. The capsule is clearly and carefully marked to indicate the up direction. For those experiments in which melting occurs, the Pt-Rh bead will sink to the bottom of the capsule, whereas for those experiments where melting does not occur, the metal bead will be supported by the crystalline material underneath it.

The melting curve for NaCl is well documented to 1.8 GPa from DTA experiments of Clark (1959) in an internally heated gas pressure vessel as well as at 4.95 ± 0.20 GPa (1457 ± 10 °C) from experiments in a multi-anvil device using in-situ X-ray radiography (Lange and Chen 2005). Bohlen (1984) additionally bracketed the NaCl melting reaction at 0.5 GPa in an internally heated pressure vessel. Lange and Chen (2005) used fusion curve analysis to calculate the NaCl melting curve from available thermodynamic data; their recommended curve matches all the experimental temperatures with an average deviation of ± 3 degrees and a maximum deviation of 8 degrees. This curve permits calculation of the NaCl melting temperature at any pressure between 0 and 5 GPa.

The results of our experiments on the melting reaction for

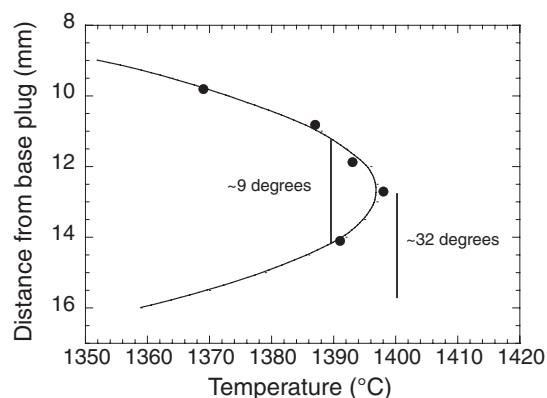


FIGURE 5. Experimentally determined thermal gradient in the pressure assembly as a function of distance from the base plug. See Tenner (2005) for detailed description of experimental procedure and results. When the hotspot is located in the center of a 3 mm capsule, the thermal gradient along the capsule length is ~ 9 °C. When the hotspot is located at top of the capsule, the thermal gradient is ~ 32 °C.

reagent grade NaCl (99.997% purity) at a nominal pressure of 2 GPa is shown in Figure 6, where the thermal gradient along the lengths of the capsules are also shown. The results indicate that the melting temperature is between 1121 and 1127 °C (1124 ± 3 °C). This corresponds to a pressure of 1.86 ± 0.02 GPa for the NaCl melting curve, which indicates a pressure correction of $-7 \pm 1\%$. For comparison, a $-9 \pm 2\%$ correction for BaCO₃ cells was reported by McDade et al. (2002) at Bristol University, and a -6% correction for BaCO₃ cells was obtained at the University of Minnesota (M. Hirschmann, personal communication). Therefore, our pressure correction is in agreement with those obtained at other laboratories.

Experiments on NaAlSi₃O₈ glass at high pressure

The NaAlSi₃O₈ glass used in the piston-cylinder experiments was synthesized and analyzed by Ochs and Lange (1997). The glass composition is close to the exact stoichiometry of NaAlSi₃O₈ as seen in the analysis (Table 3). The glass was powdered and packed into 3 mm diameter Pt capsules. The capsules were coned nearly shut and placed in a furnace for ≥ 12 h at 750 °C. After heating they were placed in a vacuum bell jar to cool. The capsules were then immediately coned shut, spot welded, and shaped into cylinders. The MgO was heated at 1000 °C for ≥ 12 h prior to experiments, and the BaCO₃ cells were stored in a 150 °C furnace before they were needed (this procedure applied to the NaCl melting experiments as well).

Experiments were brought to pressure by first raising the pressure to $\sim 90\%$ of the desired pressure before the temperature was ramped up to the desired set point. Once the final temperature was reached, the pressure was increased to its desired value.

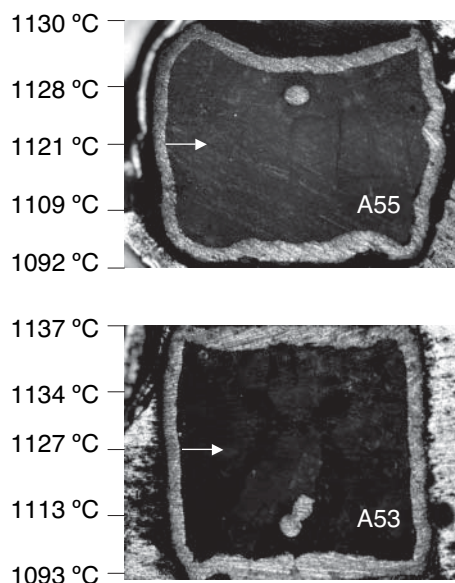


FIGURE 6. Reflected-light micrographs of cut and polished charges for two experiments that bracket the NaCl melting reaction at a nominal pressure of 2 GPa. The orientation of the capsules is that during the experiments. The thermal gradient down the length of each capsule is shown. The white arrows indicate conservative estimates of the minimum (run A55) and maximum (run 53) melting temperature of NaCl.

After the samples reached the target temperature and pressure, they were held for 40–50 min. During this time interval, there was a slow increase in pressure, even though the oil supply was shut off and no leaking was visible in the system. To keep the pressure stable, the valve on the lower ram was opened every time the pressure was 0.005 GPa above the desired value and the pressure was dropped to 0.005 GPa below the desired value. The valve was then left partially open to slow the pressure increase. This needed to be repeated five or six times over the course of each run. The same pressure conditions occurred during the NaCl pressure calibration described above.

Samples were quenched by shutting-off power to the graphite furnace. The sample capsules were retrieved, and each was cut lengthwise and polished to make a thin-section mount for viewing under plane-polarized light.

H₂O analysis of quenched NaAlSi₃O₈ glass

Run products that quenched to glass were mounted in epoxy, doubly polished, and analyzed by a Perkin-Elmer Spectrum GX Fourier Transform Infrared (FTIR) spectrometer to determine the absorbance of the samples. The water concentrations were determined with the Beer-Lambert Law equation:

$$\text{Abs}_{3570} = C_{\text{H}_2\text{O}} \cdot d \cdot \rho \cdot \epsilon_{3570} / 18.0152 \quad (5)$$

where Abs_{3570} is the absorbance at 3570 cm⁻¹ band, $C_{\text{H}_2\text{O}}$ is the weight fraction of total water, d is the sample thickness, ρ is the albite glass density, and ϵ_{3570} is the molar absorptivity. A value of 70.00 ± 2.0 L/(mol·cm) was used for the molar absorptivity (Mandeville et al. 2002). Samples ranged from 0.98–1.02 mm in thickness. It is certain that the density of the quenched NaAlSi₃O₈ glass increased with the pressure of the piston-cylinder experiments owing to compression. When all else is equal, the effect of increasing the glass density is to reduce the calculated water concentration from the Beer-Lambert Law equation. Therefore, maximum water concentrations were calculated for the glasses quenched from the piston-cylinder experiments by using the density for NaAlSi₃O₈ glass synthesized at one bar (2.376 g/cm³; Ochs and Lange 1997). The results indicate that H₂O concentrations in the quenched glasses ranged from 0.007 wt% to 0.050 wt% H₂O (70–500 ppm) (Table 4). Therefore, there was negligible contamination by water in our experiments.

Experimental results

The results of the piston-cylinder experiments are summarized in Table 4. Although experiments were conducted at three pressures (1.86 ± 0.03 , 2.33 ± 0.03 , and 2.79 ± 0.03 GPa), temperature brackets on the melting reaction were only obtained at 2.33 and 2.79 GPa. Images of several of the run products are shown in Figures 7 and 8 (from experiments at 2.33 and 2.79 GPa, respectively). The run products had two distinct textures: (1)

TABLE 3. Composition of starting glass (NaAlSi₃O₈)

Oxide	Analyzed composition		Ideal albite (mol%)
	Measured (wt%)	Normalized (mol%)	
SiO ₂	68.5	74.99	75.00
Al ₂ O ₃	19.42	12.53	12.50
Na ₂ O	11.76	12.48	12.50
H ₂ O	0.22	–	–
Total	99.68	100	100

clear glass, and (2) opaque, fine-grained crystals. For example, samples equilibrated in the liquid stability field quenched to a clear glass (e.g., top of A75 and A76 in Fig. 7; top of A72, A50, and A60 in Fig. 8). In contrast, samples equilibrated in the crystalline stability field quenched to fine-grained crystals (e.g., runs A74 and A73 and bottom of runs A75 and A76 in Fig. 7; run A54 and bottom of runs A65, A72, and A50 in Fig. 8). Only two run products deviated from these two textures. First, the top of sample A65 (Fig. 8) contains a mixture of clear glass and some

crystals as seen in cross-polarized light in Figure 9. Second, the bottom of run A57 (Fig. 8) contains significantly coarser crystals than seen in most of the other crystalline run products. Powder X-ray diffraction experiments were conducted on the crystalline material from runs A108 and A114 (Table 4), which confirmed that it is high albite.

One of the most important features shown in Figures 7 and 8 is the progression from glass to crystal seen in the run products with decreasing temperature both: (1) down the length of individual capsules (e.g., runs A75 and A76 in Fig. 7 and runs A72 and A50 in Fig. 8), and (2) from capsule to capsule with decreasing set-point temperature at each pressure. The images also demonstrate that $\text{NaAlSi}_3\text{O}_8$ readily quenches to a glass and that 40 min is sufficient time for crystallization and/or melting of albite to occur. In other words, sluggish kinetics is not a problem at these temperatures and pressures.

The results from each run product in Table 4 were used to place brackets on the melting reaction at 2.33 and 2.79 GPa as shown in Figure 10. For each run, the top and bottom of the capsule were used to place a conservative temperature bracket on the melting reaction. Both the temperature and the texture (glass or crystal) are well characterized for the top and bottom of each capsule. In Figure 10, open triangles indicate those temperatures where the bottom or top of the capsules was crystalline, whereas closed triangles indicate those temperatures where the bottom or top of the capsules was glass. In combination, the results in

TABLE 4. Experimental results for $\text{NaAlSi}_3\text{O}_8$ crystallization/melting reaction

Run no.	Pressure (calibrated) GPa	T (°C): run product Top of capsule	T (°C): run product Bottom of capsule	H ₂ O analyses wt%
A114	1.86	1300: crystal	1256: crystal	
A80	1.86	1272: crystal	1240: crystal	
A77	2.33	1378: glass	1339: crystal	
A76	2.33	1376: glass	1337: crystal	0.015
A75	2.33	1370: glass	1319: crystal	0.012
A73	2.33	1360: crystal	1324: crystal	
A74	2.33	1352: crystal	1299: crystal	
A60	2.79	1452: glass	1420: glass	0.007
A50	2.79	1402: glass	1366: crystal	0.050
A72	2.79	1389: glass	1351: crystal	0.009
A65	2.79	1385: mixed	1326: crystal	
A57	2.79	1370: crystal	1336: crystal	
A54	2.79	1340: crystal	1300: crystal	
A52	2.79	1290: crystal	1249: crystal	

Note: Values in bold represent the run results that bracket the liquid/crystal phase transition at 2.33 and 2.79 GPa.

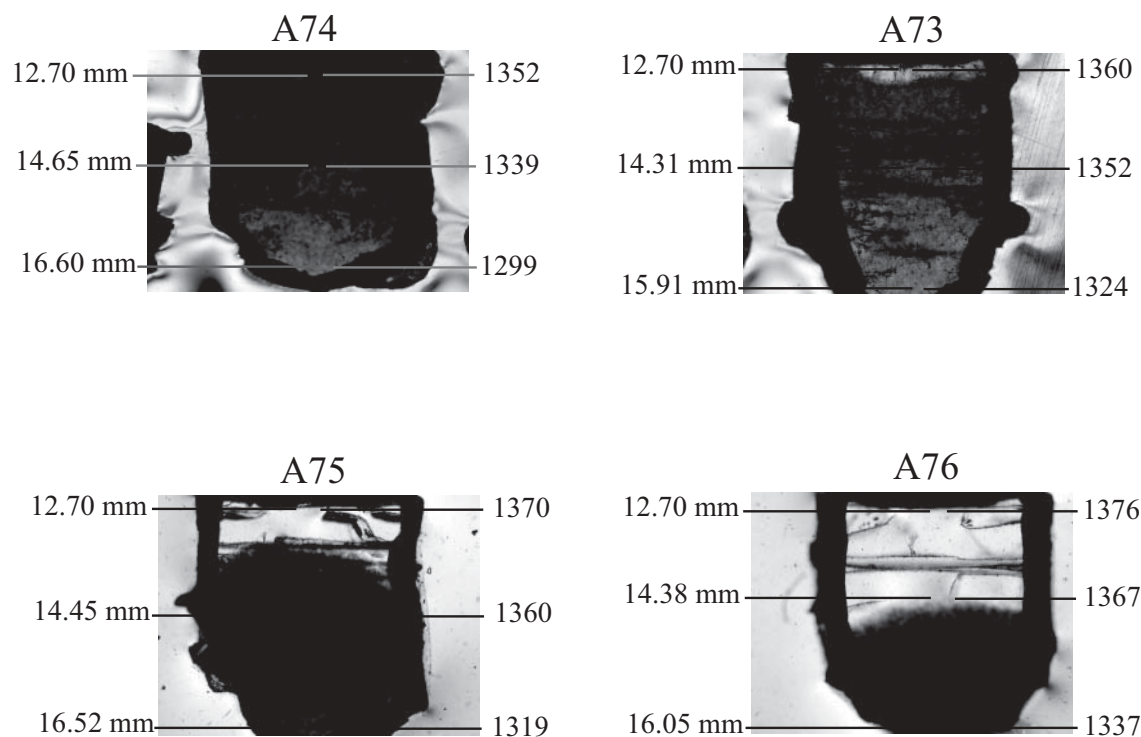


FIGURE 7. Plane polarized images of four run products from experiments at 2.33 ± 0.03 GPa experiments; the thermal gradient down the length of each capsule is shown. The orientation of the capsules is that during the experiment. At experimental temperatures in the liquid stability field, $\text{NaAlSi}_3\text{O}_8$ liquid readily quenches to a glass as seen in the clear transparent portion of the capsule (bright area in grayscale image) in run A75 (top quarter), run A76 (top half). At experimental temperatures in the crystalline stability field, fine-grained high albite is found as the run product (e.g., runs A74, A73 and bottom of runs A75 and A76).

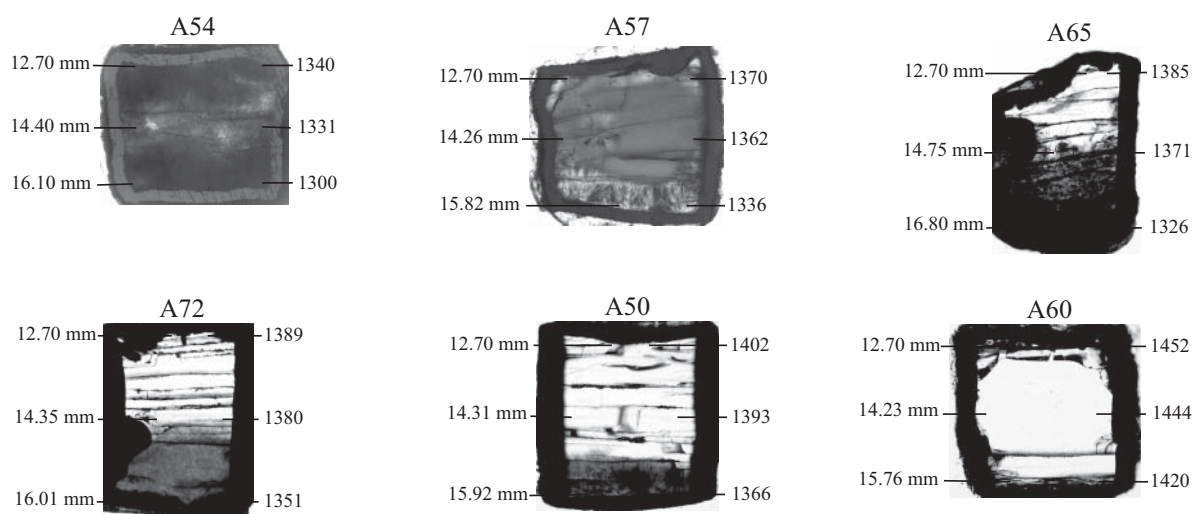


FIGURE 8. Plane polarized images of six run products from experiments at 2.79 ± 0.03 GPa; the thermal gradient down the length of each capsule is shown. The orientation of the capsules is that during the experiment. Capsules range from 3.46–3.90 mm in length. At experimental temperatures in the liquid stability field, $\text{NaAlSi}_3\text{O}_8$ liquid readily quenches to a glass as seen in the clear transparent portion (bright area in grayscale image) of the capsule in run A72 (top half), run A50 (top two-thirds), and run A60 (entire capsule). At experimental temperatures in the crystalline stability field, fine-grained high albite is found as the run product (e.g., bottom of run A72 and A50).

Table 4 and Figure 10 indicate conservative brackets on the melting reaction between 1360 and 1370 °C at 2.33 ± 0.03 GPa and between 1370 and 1389 °C at 2.79 ± 0.03 GPa.

DISCUSSION

Constraints on the K'_0 of $\text{NaAlSi}_3\text{O}_8$ liquid

The experimental results (Fig. 10) that bracket the location of the albite fusion curve in P - T space are superimposed on a family of calculated fusion curves for different K'_0 values for $\text{NaAlSi}_3\text{O}_8$ liquid, using the third-order Birch-Murnaghan EOS. The phase equilibrium experiments constrain the value for the liquid K'_0 to be 10.8 ± 0.5 . However, when the errors in the one-bar thermodynamic data are considered, the uncertainty in the liquid K'_0 increases to ± 1.5 . With this calculated fusion curve in hand, for a liquid K'_0 of 10.8 ± 1.5 , a comparison with all previous work can be made at all experimental pressures.

Comparison with previous work

A comparison between our results (Fig. 10) and those of Birch and LeComte (1960) (Fig. 11a) resolves two questions regarding their experimental data. The first is whether their no-reaction experiments at 1323 and 1358 °C for >2.5 h with a starting material of crystalline albite were a result of sluggish kinetics. Our results at temperatures ≥ 1272 °C demonstrate that albite melts and crystallizes readily within 45 min or less. Therefore, the “no-reaction” experiments of Birch and LeComte (1960) conducted at 1.99 and 2.29 GPa (both at temperatures >1300 °C), which lasted more than 2.5 h, can be confidently interpreted as P - T conditions within the crystalline stability field. The second question is whether their crystalline starting material was low or high albite. There is no evidence that the results of Birch and LeComte (1960) reflect metastable melting of low albite at temperatures lower than those for high albite.



FIGURE 9. Blow-up of experimental charge from run A65 (Fig. 8) under cross-polarized light, which shows crystals, along with glass, at the top of the capsule. The Pt capsule is approximately 3.90 mm from top to bottom.

To the contrary, the temperature brackets provided by Birch and LeComte (1960) for the albite fusion curve are among the highest in temperature compared to previous studies and match this study (where high albite was confirmed by X-ray diffraction). As an aside, the excellent agreement between the results from our study and those from Birch and LeComte (1960), which had excellent pressure control owing to the gas pressure medium, provides an independent verification on the pressure calibration of this study.

Our results are also consistent with those of Boyd and England (1963), especially when the negative 6% pressure correction for talc/BN assemblies documented by Bohlen et al. (1980) are applied to the Boyd and England results. This leads to revised pressures of 1.02 , 1.68 , 2.36 , and 3.04 GPa, for temperature brackets of 1225 – 1250 , 1300 – 1325 , 1350 – 1375 , and 1400 – 1425

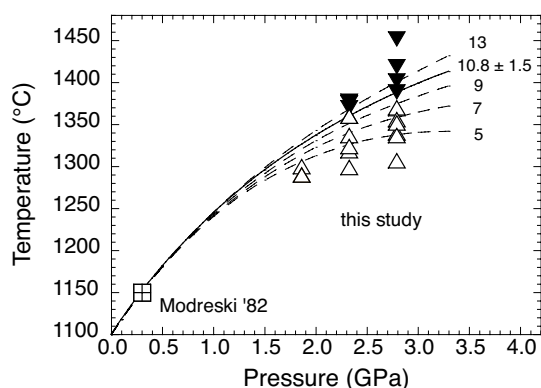


FIGURE 10. The phase equilibrium results from this study (Table 4) superimposed on the calculated fusion curve for high albite for a family of liquid K'_0 values. These calculations use the third-order Birch-Murnaghan equation of state. The solid line is for a liquid $K'_0 = 10.8$, whereas the dashed lines are values that range from 5–13.

°C, respectively, that tightly fit the fusion curve calculated for a liquid K'_0 of 10.8 ± 1.5 (Fig. 11b). The experiments of Boyd and England likely had minimal H_2O contamination, considering the short run durations (20–60 min) of their experiments and the ease with which their $NaAlSi_3O_8$ liquid quenched to a glass.

Figure 11c shows the results of Boettcher et al. (1982) superimposed on the calculated family of fusion curves; there is no liquid K'_0 value that matches their data. The results of Boettcher et al. (1982) at 2.5 and 3.0 GPa are ~ 65 and ~ 53 °C lower than calculated for the fusion curve with a liquid K'_0 of 10.8. Lange (2003) provides an equation that can be used to calculate the amount of water required to suppress the albite melting temperature a known amount. From Equation 10 in that paper, the results of Boettcher et al. (1982) at 2.5 and 3.0 GPa appear to have contained ~ 0.73 and ~ 0.95 wt% H_2O , which is consistent with the range of H_2O estimated for their samples (equilibrated for 3–24 h) on the basis of the H_2O measurements reported in Fine and Stolper (1985).

Figure 11c also shows the results of Nekvasil and Carroll (1996) at 1.13 GPa, which are ~ 35 °C lower than that calculated for the albite fusion curve with 10.8 for the liquid K'_0 value. This discrepancy may be due to small amounts of H_2O (~ 0.4 wt%) infiltrating their samples, which is plausible given their long (5 day) experiments.

The density of $NaAlSi_3O_8$ liquid as a function of pressure

With constraints on the value of K'_0 for $NaAlSi_3O_8$ liquid, its density can be calculated to high pressure with the third-order Birch-Murnaghan EOS (Eq. 2). The one-bar liquid volume, thermal expansivity and compressibility used for this calculation are listed in Table 1. The density of liquid $NaAlSi_3O_8$ from 0 to 3.3 GPa at 1500 °C is illustrated in Figure 12 along with the density of crystalline high albite. The relatively large volume of fusion at one bar ($\sim 7.6\%$) may be due, in part, to a change in topology between crystalline albite, comprised of four-membered rings of tetrahedra, and liquid $NaAlSi_3O_8$, which may contain a substantial number of six-membered rings. This inference is based on X-ray diffraction experiments of Taylor and Brown

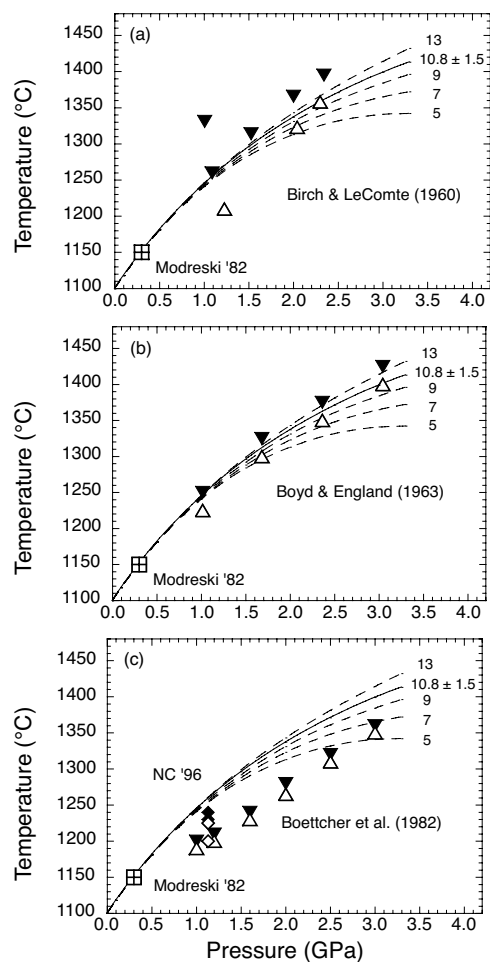


FIGURE 11. The calculated temperature of the albite melting reaction as a function of pressure to 3.3 GPa. The solid line is for a K'_0 of 10.8 ± 1.5 , which was determined from this study. The phase-equilibrium result at 0.3 GPa from the experiment of Modreski in an internally heated pressure vessel (Boettcher et al. 1982) is shown for comparison. The down-facing solid triangles denote the liquid field, whereas the up-facing open triangles denote the crystalline field. (a) Phase equilibrium experiments of Birch and LeComte (1960) in an internally heated pressure vessel. (b) Phase equilibrium experiments of Boyd and England (1963) in a piston-cylinder apparatus using talc/BN pressure assemblies; pressures have been corrected by $\sim 6\%$ based on the results from Bohlen et al. (1980). (c) Phase equilibrium experiments of Boettcher et al. (1982) in a piston-cylinder apparatus. Also shown are the experiments of Nekvasil and Carroll (1996) as solid and open diamonds (liquid and crystal, respectively) using BN/NaCl pressure assemblies.

(1979) on feldspar glasses quenched from one-bar liquids. In that study, they used X-ray radial distribution functions to infer that $NaAlSi_3O_8$ glass has a tridymite-like structure based on six-membered rings of tetrahedra, unlike the four-membered rings found in crystalline albite. Conversely, the reduced volume of fusion at 3.3 GPa ($\sim 2.7\%$) may indicate that the topology of liquid $NaAlSi_3O_8$ is changing with increasing pressure and becoming more similar to that of albite than of tridymite. This is consistent with the spectroscopic evidence from Sykes et al.

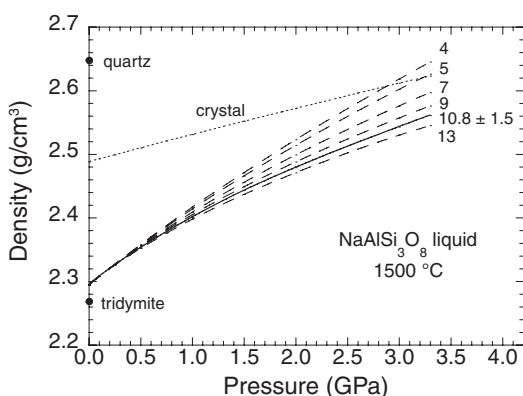


FIGURE 12. The density of $\text{NaAlSi}_3\text{O}_8$ liquid as a function of pressure at temperatures along the fusion curve. The curves are calculated with the one-bar density and compressibility results of Lange (1996) and Kress et al. (1988) and a third-order Birch-Murnaghan equation of state. The solid line is for a liquid $K'_0 = 10.8$, whereas the dashed lines are for liquid K'_0 values of 4–13. The dotted line is the calculated density of crystalline high albite at 1500 °C as a function of pressure. For comparison, the room-temperature density of tridymite and quartz (Smyth and McCormick 1995) are shown at one bar; these illustrate the large variation in density that can result from topological changes in framework structure.

(1993) on $\text{NaAlSi}_3\text{O}_8$ glasses quenched from liquids at 0, 8, and 10 GPa, where the average T-O-T bond angle decreases with increasing pressure. They also observed that the distribution of T-O-T bond angles about the mean T-O-T bond angle is reduced with pressure, which is also consistent with topological changes in the liquid structure.

The density calculated for $\text{NaAlSi}_3\text{O}_8$ liquid at 1500 °C at 3 GPa (for a liquid K'_0 of 10.8 ± 1.5) is 2.543 ± 0.010 g/cm³. The uncertainty in the liquid K'_0 value of ± 1.5 leads to an uncertainty in the liquid density at 3 GPa of only 0.4%; the error diminishes as pressure decreases. This result illustrates that fusion curve analysis can be an effective tool to obtain the density of high-pressure liquids with a remarkably high precision. There are few, if any, experimental techniques available that permit the density of such a viscous liquid as $\text{NaAlSi}_3\text{O}_8$ to be obtained at 3 GPa within <1% error.

The compressibility of $\text{NaAlSi}_3\text{O}_8$ liquid as a function of pressure

It is of interest to examine not only how the density of liquid $\text{NaAlSi}_3\text{O}_8$ varies with pressure for different K'_0 values, but also how the compressibility varies. Its variation with pressure is calculated from the equation:

$$\beta_T(P) = \frac{1}{K'_T(P)} = -\frac{1}{V_T(P)} \left[\left(\frac{\partial P}{\partial V} \right)_T \right]^{-1} \quad (6)$$

where $(\partial P/\partial V)_T$ is the derivative of Equation 2 with respect volume:

$$\left(\frac{\partial P}{\partial V} \right)_T = \frac{3}{4} \frac{K_{T,0}}{V_{T,0}} \left(R^{7/3} - R^{5/3} \right) (4 - K') R^{5/3} + \frac{3}{2} \frac{K_{T,0}}{V_{T,0}} \left(\frac{5}{3} R^{8/3} - \frac{7}{3} R^{10/3} \right) \left(1 - \frac{3}{4} (4 - K') (R^{2/3} - 1) \right) \quad (7)$$

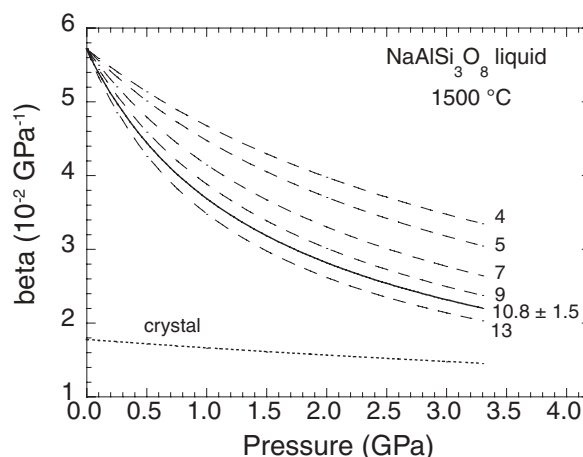


FIGURE 13. The isothermal compressibility of $\text{NaAlSi}_3\text{O}_8$ liquid as a function of pressure at 1500 °C. The curves are calculated from the one-bar density and compressibility results of Lange (1996) and Kress et al. (1988) and a third-order Birch-Murnaghan equation of state. The solid line is for a liquid $K'_0 = 10.8$, whereas the dashed lines are for liquid K'_0 values of 4–13. The dotted line is the compressibility of high albite as a function of pressure.

The resultant β_T vs. pressure curves at 1500 °C (Fig. 13) show that for a K'_0 value of 10.8 ± 1.5 at 1500 °C there is a pronounced curvature, with β_T rapidly decreasing at low pressure. In contrast, a low K'_0 value of 4 (commonly assumed for magmatic liquids) leads to a less sharp decrease in β_T with pressure. At 1500 °C, for a K'_0 value of 10.8, the liquid has a compressibility at one bar ($\sim 5.72 \times 10^{-6}$ bars⁻¹) that is >220% greater than that for crystalline albite ($\sim 1.77 \times 10^{-6}$ bars⁻¹). By 3.3 GPa, the difference between the liquid and crystalline compressibility is only 52%. These results illustrate that at one bar, there are mechanisms of compression available to liquid $\text{NaAlSi}_3\text{O}_8$ that are not accessible to its crystalline equivalent. Moreover, these mechanisms of compression are rapidly diminished with increasing pressure between 0 and 3 GPa.

Topological mechanisms of compression for liquid $\text{NaAlSi}_3\text{O}_8$

There are two broad mechanisms of compression by which the molar volume of multi-component silicate liquids may change with increasing pressure. One is topological and may involve changes in Q^n speciation, T-O-T bond angles, and network connectivity, such as the occurrence of clusters and/or changes in the size distribution of rings of tetrahedra. For example, Stixrude and Bukowinski (1990b) demonstrate that topological variations in network connectivity can exert a strong influence on melt density. Using Monte-Carlo simulations of tetrahedrally bonded SiO_2 liquid at various pressures, they showed that SiO_2 melt compresses by reducing the abundance of three-membered rings in favor of larger-sized rings and a broader distribution of the size of rings. These conclusions are consistent with the strong variations in density (factor of 2) observed in crystalline frameworks as a systematic function of ring statistics (Stixrude and Bukowinski 1990c), where >90% of the variation is caused

by topological effects and not composition. As an example, the polymorphs of SiO₂ with ^{IV}Si (tridymite, cristobalite, quartz, and coesite) illustrate that topological changes can lead to large variations in density (Fig. 12), without an increase in Si coordination. For example, at room temperature and pressure, the density of quartz (2.648 g/cm³) is ~17% higher than that of tridymite (2.269 g/cm³), which is greater than the ~12% density increase in liquid NaAlSi₃O₈ between 0 and 3.3 GPa (for liquid $K'_0 = 10.8$). Thus, as seen in Figure 12, topological changes can readily induce the magnitude of the density increase observed for NaAlSi₃O₈ liquid along its fusion curve from 0 to 3.3 GPa.

An increase in the coordination of Si⁴⁺ and Al³⁺ is another mechanism of compression for NaAlSi₃O₈ liquid at high pressure. However, although ^VAl and ^{VI}Al have been observed in NaAlSi₃O₈ glasses quenched from liquids from 8 and 10 GPa (Lee et al. 2004; Allwardt et al. 2005), these pressures are in the stability field for jadeite (with ^{VI}Al) and are well above the breakdown of albite at 3.3 GPa. Therefore, the most likely mode of compression for NaAlSi₃O₈ liquid at lower pressure (e.g., <3.5 GPa), not available to its crystalline equivalent, is one that involves changes in network topology and connectivity with increasing pressure.

CONCLUDING REMARKS

The phase equilibrium results on the fusion curve of albite presented in this study closely match the data of Birch and LeComte (1960) and the pressure corrected data of Boyd and England (1963). This study demonstrates that well-determined experimental constraints on the albite melting reaction, when combined with thermodynamic analysis of the fusion curve, allows the density and compressibility of this viscous, fully polymerized liquid to be calculated to high pressure with a remarkably high precision. A third-order Birch-Murnaghan equation of state and a K'_0 value of 10.8 ± 1.5 for liquid NaAlSi₃O₈ can be applied from 0 to ~3.5 GPa, owing to the absence of significant coordination change and the dominance of topological mechanisms of compression in this liquid over this pressure interval.

ACKNOWLEDGMENTS

We thank Eric Essene for many discussions and a review of the first draft of this paper. We also thank Marc Hirschmann and Tony Withers for discussion regarding piston-cylinder pressure calibrations. This research was supported by the National Science Foundation (EAR-0310079 and EAR-9903104). We thank the Smithsonian Institution for providing the albite sample used for the X-ray diffraction study.

REFERENCES CITED

- Agee, C.B. and Walker, D. (1993) Olivine flotation in mantle melt. *Earth and Planetary Science and Letters*, 114, 315–324.
- Allwardt, J.R., Poe, B.T., and Stebbins, J.F. (2005) The effect of fictive temperature on Al coordination in high-pressure (10 GPa) sodium aluminosilicate glasses. *American Mineralogist*, 90, 1453–1457.
- Anderson, O.L. (1995) Equation of state of solids for geophysics and ceramic science, 405 p. Oxford University Press, New York.
- Angel, R.J., Hazen, R.M., McCormick, T.C., Prewitt, C.T., and Smyth, J.R. (1988) Comparative compressibility of end-member feldspars. *Physics and Chemistry of Minerals*, 15, 313–318.
- Angel, R.J., Downs, R.T., and Finger, L.W. (2000) High-temperature–high-pressure diffraction. In R.M. Hazen and R.T. Downs, Eds., *High-Temperature and High-Pressure Crystal Chemistry*, 41, p. 559–596. Reviews in Mineralogy and Geochemistry, Mineralogical Society of America, Chantilly, Virginia.
- Anovitz, L.M. and Blencoe, J.G. (1999) Dry melting of albite. *American Mineralogist*, 84, 1830–1842.
- Berman, R.G. (1988) Internally consistent thermodynamic data for minerals in the system Na₂O-K₂O-CaO-MgO-FeO-Fe₂O₃-Al₂O₃-SiO₂-TiO₂-H₂O-CO₂. *Journal of Petrology*, 29, 445–522.
- Birch, F. (1978) Finite strain isotherm and velocities for single-crystal and polycrystalline NaCl at high pressure and 300 K. *Journal of Geophysical Research*, 83, 1257–1268.
- Birch, F. and LeComte, P. (1960) Temperature-pressure plane for albite composition. *American Journal of Science*, 258, 209–217.
- Boettcher, A.L., Burnham, C.W., Windom, K.E., and Bohlen, S.R. (1982) Liquids, glasses and the melting of silicates to high pressures. *The Journal of Geology*, 90, 127–138.
- Bohlen, S.R. (1984) Equilibria for precise pressure calibration and a frictionless furnace assembly for the piston-cylinder apparatus. *Neues Jahrbuch für Mineralogie. Monatshefte*, 4, 404–412.
- Bohlen, S.R., Essene, E.J., and Boettcher, A.L. (1980) Reinvestigation and application of olivine-quartz-orthopyroxene barometry. *Earth and Planetary Science Letters*, 47, 1–10.
- Boyd, F.R. and England, J.L. (1963) Effect of pressure on the melting of diopside, CaMgSi₂O₆, and albite NaAlSi₃O₈, in the range up to 50 kilobars. *Journal of Geophysical Research*, 68, 311–323.
- Clark, S.P. (1959) Effect of pressure on the melting points of eight alkali halides. *Journal of Chemical Physics*, 31, 1526–1531.
- Downs, R.T., Hazen, R.M., and Finger, L.W. (1994) The high-pressure crystal chemistry of low albite and the origin of the low pressure dependency of Al-Si ordering. *American Mineralogist*, 79, 1042–1052.
- Fei, Y. (1995) Thermal expansion. In T. Ahrens, Ed., *Mineral Physics and Crystallography*, p. 29–44. AGU Reference shelf 2, Washington, D.C.
- Fine, G. and Stolper, E. (1985) The speciation of carbon dioxide in sodium aluminosilicate glasses. *Contributions to Mineralogy and Petrology*, 91, 105–121.
- Hackwell, T.P. (1993) Feldspars at high pressures and temperatures. Ph.D. thesis, University of London, U.K.
- Hackwell, T.P. and Angel, R.J. (1992) Compressibilities of boron-feldspars and their aluminum analogues. *European Journal of Mineralogy*, 4, 1221–1227.
- Hemingway, B.S., Krupka, K.M., and Robie, R.A. (1981) Heat capacities of the alkali feldspars between 350 and 1000 K from differential scanning calorimetry, the thermodynamic functions of the alkali feldspars from 298.15 to 1400 K, and the reaction quartz + jadeite = analbite. *American Mineralogist*, 66, 1202–1215.
- Holland, T.J.B. (1980) The reaction albite = jadeite + quartz determined experimentally in the range 600–1200 °C. *American Mineralogist*, 65, 129–134.
- King, H.E. and Finger, L.W. (1979) Diffracted beam crystal centering and its application to high-pressure crystallography. *Journal of Applied Crystallography*, 12, 374–378.
- Kress, V.C., Williams, Q., and Carmichael, I.S.E. (1988) Ultrasonic investigation of melts in the system Na₂O-Al₂O₃-SiO₂ liquids between 701 and 1896 K: extension to crustal magmatic temperatures. *Contributions to Mineralogy and Petrology*, 130, 1–11.
- Krupka, K.M., Robie, R.A., and Hemingway, B.S. (1979) High-temperature heat capacities of corundum, periclase, anorthite, CaAl₂Si₂O₈ glass, muscovite, pyrophyllite, KaAlSi₃O₈ glass, grossular, and NaAlSi₃O₈ glass. *American Mineralogist*, 64, 86–101.
- Lange, R.A. (1996) Temperature independent thermal expansivities of sodium aluminosilicate melts between 713 and 1835 K. *Geochimica et Cosmochimica Acta*, 60, 4989–4996.
- (2003) The fusion curve of albite revisited and the compressibility of NaAlSi₃O₈ liquid with pressure. *American Mineralogist*, 88, 109–120.
- (2007) The density and compressibility of KAlSi₃O₈ liquid to 6.5 GPa. *American Mineralogist*, 92, 114–123.
- Lange, R.A. and Chen, J. (2005) The NaCl fusion curve: new experiments to 5 GPa and constraints on the liquid equation of state. *American Geophysical Union, Transactions, Fall meeting, Abstract MR13A-0064*.
- Lee, S.K., Cody, G.D., Fei, Y., and Mysen, B.O. (2004) Nature of polymerization and properties of silicate melts and glasses at high pressure. *Geochimica et Cosmochimica Acta*, 68, 4189–4200.
- Mandeville, C.W., Webster, J.D., Rutherford, M.J., Taylor, B.E., Timbal, A., and Faure, K. (2002) Determination of molar absorptivities for infrared absorption bands of H₂O in andesitic glasses. *American Mineralogist*, 87, 813–821.
- Mao, H.K., Bell, P.M., Shaner, J.W., and Steinberg, D.J. (1978) Specific volume measurements of Cu, Mo, Pd, and Ag and calibration of the ruby R₁ fluorescence pressure gauge from 0.06 to 1 Mbar. *The Journal of Applied Physics*, 49, 3276–3283.
- McDade, P., Wood, B.J., Van Westrenen, W., Brooker, R., Gudmundsson, G., Soular, H., Najorka, J., and Blundy, J. (2002) Pressure corrections for a selection of piston-cylinder cell assemblies. *Mineral Magazine*, 66, 1021–1028.
- Navrotsky, A., Hon, R., Weill, D.R., and Henry, D.J. (1980) Thermochemistry of glasses and liquids in the systems CaMgSi₂O₆-CaAl₂Si₂O₈-NaAlSi₃O₈, SiO₂-CaAl₂Si₂O₈-NaAlSi₃O₈, and SiO₂-Al₂O₃-CaO-Na₂O. *Geochimica et Cosmochimica Acta*, 44, 1409–1423.
- Nekvasil, H. and Carroll, W. (1996) Experimental constraints on the compositional evolution of crustal magmas. *Transactions of the Royal Society of Edinburgh*:

- Earth Sciences, 87, 139–146.
- Ochs III, F.A. and Lange, R.A. (1997) The partial molar volume, thermal expansivity, and compressibility of H₂O in NaAlSi₃O₈ liquid: new measurements and an internally consistent model. *Contributions to Mineralogy and Petrology*, 129, 155–165.
- Richet, P. (1987) Heat capacity of silicate glasses. *Chemical Geology*, 62, 111–124.
- Richet, P. and Bottinga, Y. (1984) Glass transitions and thermodynamic properties of amorphous SiO₂, NaAlSi₃O₈ and KAlSi₃O₈. *Geochimica et Cosmochimica Acta*, 48, 453–470.
- Rigden, S.M., Ahrens, T.J., and Stolper, E.M. (1989) High-pressure equation of state of molten anorthite and diopside. *Journal of Geophysical Research*, 92, 9508–9520.
- Robie, R.A., Hemingway, B.S., and Wilson, W.H. (1978) Low temperature heat capacities and entropies of feldspar glasses and anorthite. *American Mineralogist*, 63, 109–123.
- Smith, J.V. and Brown, W.L. (1988) *Feldspar Minerals 1. Crystal Structures, Physical, Chemical, and Microtextural Properties*, 828 p. Springer-Verlag, New York.
- Smyth, J.R. and McCormick, T.C. (1995) Crystallographic data for minerals. In T. Ahrens, Ed., *Mineral Physics and Crystallography*, p. 1–17. AGU Reference shelf 2, Washington, D.C.
- Stebbins, J.F., Weill, D.E., Carmichael, I.S.E., and Moret, L.K. (1982) High temperature heat contents and heat capacities of liquids and glasses in the system NaAlSi₃O₈-CaAl₂Si₂O₈.
- Stebbins, J.F., Carmichael, I.S.E., and Weill, D.E. (1983) The high temperature liquid and glass heat contents and heats of fusion of diopside, albite, sanidine and nepheline. *American Mineralogist*, 68, 717–730.
- Stixrude, L. and Bukowinski, M.S.T. (1990a) Fundamental thermodynamic relations and silicate melting with implications for the constitution of D". *Journal of Geophysical Research*, 95, 19311–19327.
- (1990b) A novel topological compression mechanism in a covalent liquid. *Science*, 250, 541–543.
- (1990c) Rings, topology, and the density of tectosilicates. *American Mineralogist*, 75, 1159–1169.
- Sykes, D., Poe, B.T., McMillan, P.F., Luth, R.W., and Sato, R.K. (1993) A spectroscopic investigation of anhydrous KAlSi₃O₈ and NaAlSi₃O₈ glasses quenched from high pressure. *Geochimica et Cosmochimica Acta*, 57, 1753–1759.
- Taylor, M. and Brown, G.E. (1979) Structure of mineral glasses: I. The feldspar glasses NaAlSi₃O₈, KAlSi₃O₈, CaAl₂Si₂O₈. *Geochimica et Cosmochimica Acta*, 43, 61–75.
- Tenner, T.J. (2005) The albite fusion curve re-examined: new experiments and the density and compressibility of NaAlSi₃O₈ liquid with pressure. M.S. thesis, University of Michigan.
- Tuttle, O.F. and Bowen, N.L. (1958) Origin of granite in the light of experimental studies in the NaAlSi₃O₈-KAlSi₃O₈-SiO₂-H₂O. *Geological Society of America Memoir*, 74, 1–153.

MANUSCRIPT RECEIVED SEPTEMBER 27, 2006

MANUSCRIPT ACCEPTED MAY 21, 2007

MANUSCRIPT HANDLED BY MARTIN KUNZ